MOLECULAR AND CELLULAR BIOLOGY, Aug. 2004, p. 6919–6930 Vol. 24, No. 16
0270-7306/04/$08.00+0 DOI: 10.1128/MCB.24.16.6919–6930.2004

Biochemical and Phenotypic Abnormalities in Kynurenine Aminotransferase II-Deficient Mice

Ping Yu,[1]† Nicholas A. Di Prospero,[1]‡ Michael T. Sapko,[2] Tao Cai,[3] Amy Chen,[1] Miguel Melendez-Ferro,[2] Fu Du,[2] William O. Whetsell, Jr.,[4] Paolo Guidetti,[2] Robert Schwarcz,[2] and Danilo A. Tagle[1]*

Genetics and Molecular Biology Branch, National Human Genome Research Institute,[1] and Experimental Medicine Section, Oral Infection and Immunity Branch, National Institute of Dental and Craniofacial Research,[3] National Institutes of Health, Bethesda, Maryland 20892; Maryland Psychiatric Research Center, University of Maryland School of Medicine, Baltimore, Maryland 21228[2]; and Department of Pathology, Vanderbilt University Medical Center, Nashville, Tennessee 37235[4]

Received 23 February 2004/Returned for modification 23 March 2004/Accepted 26 May 2004

Kynurenic acid (KYNA) can act as an endogenous modulator of excitatory neurotransmission and has been implicated in the pathogenesis of several neurological and psychiatric diseases. To evaluate its role in the brain, we disrupted the murine gene for kynurenine aminotransferase II (KAT II), the principal enzyme responsible for the synthesis of KYNA in the rat brain. *mKat-2*$^{-/-}$ mice showed no detectable KAT II mRNA or protein. Total brain KAT activity and KYNA levels were reduced during the first month but returned to normal levels thereafter. In contrast, liver KAT activity and KYNA levels in *mKat-2*$^{-/-}$ mice were decreased by >90% throughout life, though no hepatic abnormalities were observed histologically. KYNA-associated metabolites kynurenine, 3-hydroxykynurenine, and quinolinic acid were unchanged in the brain and liver of knockout mice. *mKat-2*$^{-/-}$ mice began to manifest hyperactivity and abnormal motor coordination at 2 weeks of age but were indistinguishable from wild type after 1 month of age. Golgi staining of cortical and striatal neurons revealed enlarged dendritic spines and a significant increase in spine density in 3-week-old *mKat-2*$^{-/-}$ mice but not in 2-month-old animals. Our results show that gene targeting of *mKat-2* in mice leads to early and transitory decreases in brain KAT activity and KYNA levels with commensurate behavioral and neuropathological changes and suggest that compensatory changes or ontogenic expression of another isoform may account for the normalization of KYNA levels in the adult *mKat-2*$^{-/-}$ brain.

The kynurenine pathway, which constitutes the main mode of tryptophan degradation in most mammalian cells (Fig. 1), contains several neuroactive metabolites. One branch of the catabolic cascade produces two neurotoxic compounds, 3-hydroxykynurenine and quinolinic acid. The latter is an agonist of the *N*-methyl-D-aspartate (NMDA) receptor (61) and is a potent excitotoxin (55), while 3-hydroxykynurenine can cause neuronal death because of its ability to generate free radicals (14, 40). These two molecules can act synergistically to cause neurodegeneration in vivo (22) and in vitro (10). Moreover, there is accumulating evidence for the involvement of both quinolinic acid and 3-hydroxykynurenine in the pathogenesis of the AIDS-dementia complex (26, 50), Huntington's disease (21, 23, 44), schizophrenia (54), and several other human brain disorders (59).

The other branch of the kynurenine pathway (Fig. 1) produces a neuroinhibitory compound, kynurenic acid (KYNA), which has anticonvulsant and neuroprotective properties (17, 37, 64) and is of recent interest for the development of treatments for epilepsy, traumatic brain injury, and stroke (reviewed in reference 59). In the high micromolar range, KYNA blocks all ionotropic glutamate receptors, but it preferentially antagonizes the glycine coagonist site of the NMDA receptor at lower concentrations (31, 46). Recently, KYNA was also shown to potently inhibit α7 nicotinic acetylcholine receptor (α7nAChR) function (28).

Control mechanisms for the release of newly produced KYNA into the extracellular compartment have so far not been identified (63). However, KYNA formation is influenced by the availability of 2-oxoacids (30), by cellular energy status (7, 18, 29, 63), and by dopaminergic activity (47, 49, 67). Some of these regulatory processes are brain specific. Moreover, brain KYNA levels are abnormal in diseases such as Huntington's disease (4, 21, 69) and schizophrenia (15, 54), and evidence suggests that relatively modest variations in brain KYNA, acting as an endogenous modulator of glutamatergic and cholinergic neurotransmission, may be functionally significant.

KYNA is produced enzymatically by irreversible transamination of kynurenine, the primary catabolic product of tryptophan, and the newly formed KYNA is secreted into the extracellular milieu (58, 62, 63). In rats, cerebral KYNA biosynthesis is catalyzed by two kynurenine aminotransferases (KAT I and II) (41), both of which are preferentially contained in nonneuronal cells (9). KAT I, which is identical with glutamine aminotransferase K (EC 2.6.1.64) (1, 38), converts kynurenine most effectively at basic pH and is potently inhibited by physiological concentrations of glutamine and other abundant amino acids. In contrast, KAT II (L-α-aminoadipate aminotransferase; EC 2.6.1.40) has a pH optimum of 7.4, is not inhibited by common amino acids, and has therefore been

* Corresponding author. Present address: National Institute of Neurological Disorders and Stroke, Neuroscience Center, Rm. 2133, NIH, 6001 Executive Blvd., Bethesda, MD 20892. Phone: (301) 496-5745. Fax: (301) 402-1501. E-mail: tagled@ninds.nih.gov
† Present address: NCI—Frederick, Frederick, MD 21702.
‡ Present address: NINDS, NIH, Bethesda, MD 20892.

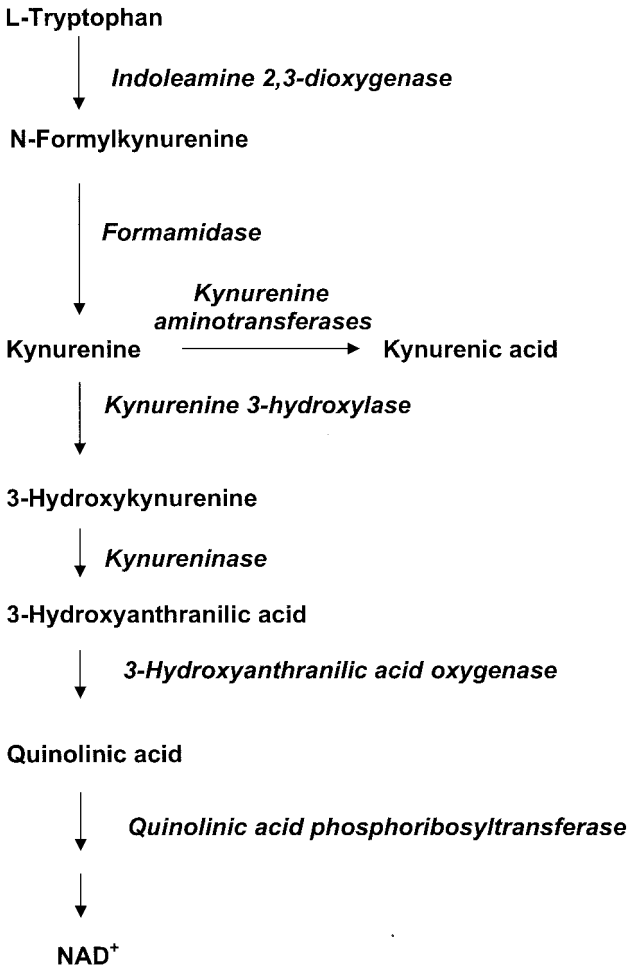

FIG. 1. Kynurenine pathway of tryptophan degradation.

postulated to function as the major determinant of KYNA production in the brain (20).

Pharmacological tools exist to manipulate the quinolinate branch of the kynurenine pathway and thus enhance the brain levels of KYNA (45, 53), but no agents are currently available to specifically inhibit KAT activity and thus reduce brain KYNA. To investigate the role of KAT II in KYNA synthesis in the mouse brain and to examine consequent behavioral and pathological abnormalities caused by decreased KYNA levels, we disrupted the *Kat-2* gene in mice by homologous recombination. We report here that mice lacking the *mKat-2* gene show a perinatal reduction in brain KYNA levels that is accompanied by behavioral and pathological abnormalities. However, these changes were transitory, and improvement by 1 month of age was concomitant with full restoration of cerebral KYNA levels. Our results suggest additional mechanisms which may regulate brain KYNA levels in adult mice.

MATERIALS AND METHODS

Chemicals. *tert*-Butylammonium hydrogen sulfate (TBAS) was purchased from Fluka Chemika (Buchs, Switzerland). Unless stated otherwise, all biochemicals, including avertin, were obtained from Sigma-Aldrich Chemical Company (St. Louis, Mo.). Acids and solvents (p.a. grade) were purchased from various commercial suppliers.

Gene targeting and generation of KAT II-deficient mice. The mouse *Kat-2* sequence and genomic organization were determined from BAC clones made from a 129/SVJ genomic library (69). The targeting construct consisted of a 5.9-kb BamHI/HindIII restriction fragment (Fig. 2A) wherein a PGKneo cassette was used to replace the KpnI/BamHI fragment (768 bp) that included exon 2 of the *mKat-2* gene. Embryonic stem (ES) cells were transfected by electroporation with the linearized targeting construct. The targeted ES cell clones were identified by Southern blotting using N-terminal flanking probes (Fig. 2A). A total of 284 G418- and fialuridine-resistant clones were screened by Southern blotting, and of the 4 positive clones obtained, 2 were injected into C57BL/6 blastocysts and implanted in Swiss Webster pseudopregnant mothers. Male chimeras were mated with Black Swiss or 129Sv/Ev females to generate heterozygous mice in a mixed or completely inbred background, respectively. Heterozygous mice were intercrossed to produce *mKat-2*$^{-/-}$ mice at a Mendelian ratio (25%; $n = 128$). The following primer pairs (Fig. 2A) were used for PCR screening and for the determination of the genotype: P1, 5′-ACA TGC TCG GGT TTG GAG AT-3′, and P3, 5′-AAG CTT TGG AAC TCA GTG GG-3′; P2, 5′-GTG GAT GTG GAA ATG TGT GTG CG-3′, and P4, 5′-GAG ACA GAC ACC TTG ATA CT-3′. The PCR mixture (15 μl total) contained 50 ng of mouse tail DNA, 7.5 μl of MasterAmp 2× PCR PreMixes buffer (Epicentre Technologies, Madison, Wis.), 5 pmol of each primer, and 0.2 U of *Taq* DNA polymerase (Roche, Indianapolis, Ind.). PCR amplification was conducted using standard protocols, i.e., 2 min of denaturation followed by 25 cycles of 40 s of denaturation at 94°C, 40 s of annealing at 58°C, and 1 min of extension at 72°C.

Animals. 129SvEvTac mice (Taconic, Germantown, N.Y.) and NIH Black Swiss mice were used in the breedings. *mKat-2*$^{-/-}$ and wild-type mice from these pairings served as the breeders for subsequent generations. *mKat-2*$^{-/-}$ mice used in this study were bred into the 129SvEv line for four to five generations. Mice were maintained in an Association for Assessment and Accreditation of Laboratory Animal Care-approved animal facility on a 12-h light-dark cycle, with food and water available ad libitum.

Northern blot and RT-PCR analyses. For Northern blot analyses, total RNA from kidneys of 2-month-old *mKat-2*$^{-/-}$, mKat-2$^{+/-}$, and *mKat-2*$^{+/+}$ littermates was extracted according to the manufacturer's protocol (Gibco BRL, Gaithersburg, Md.). Ten micrograms of total RNA was electrophoresed and transferred to nitrocellulose membrane. The membrane was probed with α-^{32}P-labeled full-length *mKat-2* cDNA in preHYB/HYB buffer (Quality Biological Inc., Gaithersburg, Md.), washed under high-stringency conditions (0.2× SSC [1× SSC is 0.15 M NaCl plus 0.015 M sodium citrate] at 65°C), and subjected to autoradiography at −70°C. For reverse transcription-PCR (RT-PCR) analyses, total RNA ($n = 3$ for each time point) from brains and livers of 7-, 14-, 21-, 28-, and 60-day-old *mKat-2*$^{+/+}$ and wild-type mice were extracted using an RNeasy minikit (QIAGEN, Valencia, Calif.). RT-PCR was conducted on isolated RNA samples using the Clontech RT-PCR kit (Palo Alto, Calif.) for 24 cycles of amplification. The following primers were used for RT-PCR: *mKat-1* forward, 5′-ATC ATG AAG CAC CTG CGG AC-3′, and reverse, 5′-GAT AAG GCA CAG CTG AGG TC-3′; *mKat-2* forward, 5′-GTT CTC CAC ACA CAA GTC TC-3′, and reverse, 5′-GGA TCC ATC CTG TCA GTC A-3′. The expected product sizes are 530 and 625 bp, respectively, for *mKat-1* and *mKat-2*.

Protein isolation and Western analyses. Tissue homogenates from kidneys of 2-month-old *mKat-2*$^{-/-}$, mKat-2$^{+/-}$, and *mKat-2*$^{+/+}$ littermates were isolated for protein extraction. Western blot analysis was performed using a peptide-specific polyclonal antibody as described elsewhere (69), while a different polyclonal antibody (42) was used for immunoprecipitation experiments.

Behavioral analyses. Postnatal day (PND) 1 to 14, pregnant mice were checked twice daily (at 0900 to 1000 h and 1800 to 1900 h) for the presence of newborn pups. Following birth, the litters were culled to a maximum of eight pups to prevent growth or developmental differences due to litter size. On PND 1, pups were tattooed on their tails (AIMS IIIA tattoo identification system; Animal Identification and Marking Systems, Budd Lake, N.J.) in order to monitor individual developmental milestones. Beginning on PND 1, each animal was weighed and the following behavioral milestones were examined daily: (i) surface righting (the time it takes a pup that is placed on its back to return to the prone position with all four paws touching the surface); (ii) rooting (the first time the pup turns its head toward the side which has been stroked with a wisp of cotton); (iii) negative geotaxis (the time it takes a pup placed head down on a 45° angle to turn around and crawl up the slope); (iv) cliff aversion (the time it takes a pup positioned with its snout and forepaws over the edge of a structure to turn and crawl away); (v) forelimb grasping (the ability to grasp a thin rod and remain suspended for 2 s); (vi) auditory startle (involuntary movement when a small metal object is dropped onto a metallic surface 30 cm from the animal); (vii) eye opening (the first day both eyes are open); (viii) open field (the time it takes a pup placed in the center of a 30-cm-diameter circle to move outside the circle);

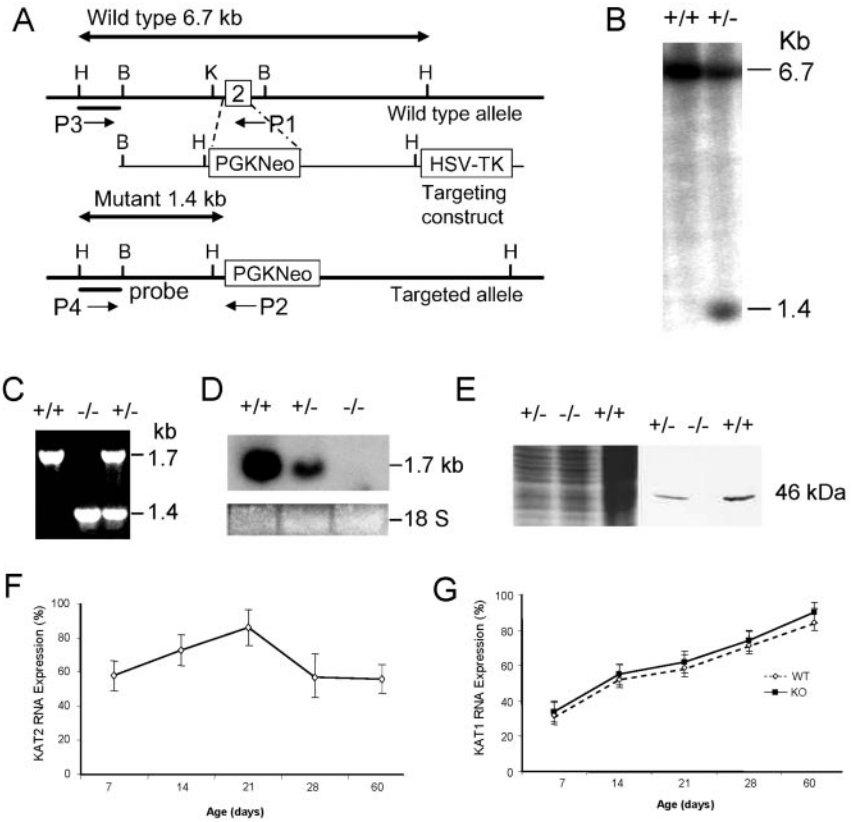

FIG. 2. Disruption of the *mKat-2*$^{-/-}$ gene by homologous recombination. (A) Strategy used for disruption of *mKat-2*. Targeting vector pPNT contained a 5.9-kb genomic sequence of the *mKat-2* genomic locus. PGKneo was ligated at KpnI (K) and BamHI (B) sites in the first and second introns of *mKat-2*$^{-/-}$, such that 1.3 kb of the 5′ and 4.6 kb of the 3′ sequences were the targeted sequences. The *mKat-2* sequences were flanked by the *TK* genes. Homologous recombination within *mKat-2* would replace the endogenous exon 2 with *PGKneo*, resulting in a frameshift downstream of the targeted region. The probe for the Southern blot assay and the primers for PCR are indicated. (B) Southern blot analysis demonstrated successful targeting using a 5′-flanking probe as indicated in panel A. The insertion of an extra HindIII site in the targeted locus produced a 1.4-kb band, while the wild type is 6.7 kb. (C) Genotype was determined by PCR method using the two primer pairs P1 and P3 for wild-type animals (PCR product size of 1.7 kb) and P2 and P3 for mutant mice (PCR product size of 1.4 kb) as indicated in panel A. (D) Northern blot analysis using full-length *mKat-2*$^{-/-}$ cDNA as probe demonstrated loss of *mKat-2*$^{-/-}$ transcripts in *mKat-2*$^{-/-}$ animals. The amount of total RNA loaded on each lane was indicated by the 18S rRNA. (E) Immunoblotting of mouse kidney homogenate using an antibody generated from peptide in exon 6 of *mKat-2*$^{-/-}$. (F) *mKat-2* expression levels during development as determined by RT-PCR from wild-type brain. Expression levels peaked at day 21. (G) Comparison of *mKat-1* developmental expression levels in mouse brain. Expression patterns were not significantly different in brain and liver (data not shown) of wild-type (open symbol) compared to *mKat-2*$^{-/-}$ (close symbol) mice, indicating that there was no augmentation of *Kat-1* expression in the *Kat-2* null background.

and (ix) air righting (the ability of a pup to land in a prone position after being dropped with its ventral side up from a height of 50 cm). A response was considered positive if the same pup was observed to perform or exhibit the behavior on two consecutive days, and all timed responses were limited to a maximum of 30 s. This test battery is based on developmental milestones (27) and provides an assessment of simple and complex tasks.

Older animals. *mKat-2*$^{-/-}$ and wild-type mice (matched for age, body weight, and gender; $n = 10$ per group) were assessed for behavioral changes by using a test battery that included the assessment of general health and gross neurological function (13). In order to identify general behavioral abnormalities (seizures, lethargy, circling, etc.) and to quantify locomotor activity, mice were placed in an open-field arena (35 by 42 cm) and videotaped for a period of 5 min. The floor of the arena was divided into 7-cm^2 sectors, and locomotor activity was quantified by a blinded observer as the number of sector crossings during the 5-min session. To further quantitate rearing behavior in these mice, a DigiScan animal activity monitor (AccuScan Instruments, Inc., Columbus, Ohio) was used ($n = 8$ per group). Mice were examined individually for 5 min in the open field, i.e., a standard photocell-equipped plexiglass box. Behavioral data, including measures of horizontal and vertical activity, total distance traversed, time spent in the center versus the perimeter of the open field, and total time spent immobile, were collected automatically.

Sensorimotor coordination was tested as described by Shi et al. (56) by using a rotarod apparatus (Bioscore Instruments, Finleyville, Pa.). Mice were placed on a 3-cm-diameter rod that was suspended 50 cm above the bottom of the apparatus. The rod accelerated linearly from 0 to 40 rpm over 2.5 min. Animals received three training runs each 30 min apart on the first day of the study and were tested on three consecutive days for three trials each day. The latencies to fall from the rod were averaged from the three trials.

Blood chemistry. Animals were anesthetized, and a heparinized wide-bore (1.0-mm) microhematocrit capillary tube was used to penetrate the orbital sinus along the lateral canthus of the eye. Approximately 200 to 300 μl of whole blood was collected in a sterile 1.5-ml Eppendorf tube, and the samples were allowed to stand at room temperature for approximately 30 min to allow the blood to clot. The samples were then centrifuged at 1,000 × *g* for 10 min at 4°C. The supernatant serum was carefully transferred to another sterile Eppendorf tube, immediately frozen in liquid nitrogen, and stored at −70°C. The samples were then shipped on dry ice to AniLytics Inc. (Gaithersburg, Md.), where routine analysis of blood chemistry was performed.

Enzyme activity and metabolite levels. (i) Measurement of KAT activity. Mice were sacrificed, and their brains and livers were harvested and stored on ice. The tissues were suspended (1:10, wt/vol) in distilled water and sonicated. The homogenates were dialyzed overnight at 4°C against 4 liters of 5 mM Tris-acetate

buffer (pH 8.0) containing 50 μM pyridoxal-5′-phosphate and 10 mM 2-mercaptoethanol. KAT activity was assessed in a 200-μl reaction mixture containing 150 mM Tris-acetate buffer (pH 7.4), 2 μM (2.5 nCi) [^{3}H]kynurenine (Amersham Corp., Arlington Heights, Ill.), 1 mM pyruvate, 80 μM pyridoxal-5′-phosphate, and 80 μl of dialysate. Liver dialysate was additionally diluted (1:25, vol/vol) prior to incubation. Samples were incubated (liver, 2 h; brain, 20 h) at 37°C, and the reaction was terminated by adding 14 μl of 50% (wt/vol) trichloroacetic acid. One milliliter of 0.1 M HCl was added, and the denatured protein was removed by centrifugation in a microcentrifuge. One milliliter of the resulting supernatant was added to a Dowex 50W H+ cation exchange column. After successive washes with 1 ml of 0.1 M HCl and 1 ml of distilled water, [^{3}H]KYNA was eluted from the column with two 1-ml volumes of distilled water and quantified by liquid scintillation spectrometry.

KAT II was precipitated using 1 μl of polyclonal anti-KAT II antibody (42) mixed with 100 μl of the dialyzed tissue homogenate and incubated at room temperature for 1 h. One milligram of insoluble protein A in 10 μl of water was then added, and the mixture was vigorously stirred and incubated at room temperature for an additional hour. Samples were centrifuged (12,000 × *g*; 10 min), and KAT activity was measured in the supernatant as described above. In all cases, blank values were obtained using samples containing heat-inactivated dialysate.

(ii) KYNA measurement. Tissues were suspended in ultrapure water (brain, 1:10 [wt/vol]; liver, 1:100 [wt/vol]) and sonicated. Five hundred microliters of the homogenate was combined with 125 μl of 5 N HCl and 500 μl of chloroform, mixed vigorously, and centrifuged (10 min; 12,000 × *g*). Twenty microliters of a 50 nM KYNA solution was added to duplicate samples as an internal standard. Five hundred microliters of the supernatant was applied to a Dowex H^+ cation exchange resin, and the column was washed successively with 200 μl of 1 N HCl, 500 μl of ultrapure water, and 500 μl of 50% methanol. KYNA was eluted with two 1-ml volumes of 50% methanol, 50 μl of TBAS was added to the eluate, and the mixture was lyophilized. The samples were reconstituted with 300 μl of distilled water, and 200 μl was subjected to high-performance liquid chromatography (HPLC) analysis. The HPLC column (HR-80; ESA, Chelmsford, Mass.) was perfused isocratically at 1 ml/min using a mobile phase consisting of 5% acetonitrile, 250 mM zinc acetate, and 50 mM sodium acetate (pH 6.2). KYNA was determined in the eluate by fluorescence detection (excitation wavelength, 344 nm; emission wavelength, 398 nm) (62).

(iii) Kynurenine and quinolinic acid measurements. Tissues were suspended in ultrapure water (brain, 1:25 [wt/vol]; liver, 1:50 [wt/vol]) and sonicated. Fifty microliters of the homogenate was combined with 50 μl of a solution containing 200 nM homophenylalanine and 100 nM 3,5-pyridinedicarboxylic acid as internal standards. The samples were then combined with 25 μl of 5 N HCl and 125 μl of chloroform, thoroughly mixed, and centrifuged (10 min; 12,000 × *g*). One hundred microliters of the supernatant was combined with 50 μl of 62.5 mM TBAS and lyophilized. The dried pellets were resuspended in 25 μl of methylene chloride containing 7.5% diisopropylethylamine and 3% pentafluorobenzylbromide (PFB-Br). The samples were incubated in sealed tubes for 15 min at 60°C. Fifty microliters of decane and 750 μl of ultrapure water were then added, and the samples were vigorously mixed and centrifuged (15 min; 7,000 × *g*). One microliter of the organic phase was injected into a gas chromatograph-mass spectrometer (GC/MS). A trace GC was used in series with a trace MS quadrupole (ThermoFinnigan, San Jose, Calif.). Chromatographic separation was achieved using a 30-m DB-5 MS capillary column with a 0.25-mm internal diameter and 0.25-μm film thickness (Alltech, Deerfield, Ill.) with helium as the carrier gas. A split-splitless injection port (1-μl injection volume) was used with a port temperature of 228°C. The temperature was programmed as follows: 155°C for 1.25 min, 40°C/min to 270°C, 10°C/min to 320°C, and 1 min at 320°C. Analysis was performed using electron capture negative-ion chemical ionization MS with methane as the reagent gas. The ion source temperature was 220°C. Selected ion monitoring analyses were performed by recording signals of characteristic $(M\text{-}PFB)^-$ ions. The *m*/*z* value was 346 for $(QUIN\text{-}PFB)^-$ and 387 for $(KYN\text{-}PFB)^-$.

(iv) 3-Hydroxykynurenine measurement. Brain or liver samples were suspended in ultrapure water (1:10, wt/vol) and sonicated. Thirty microliters of 6% perchloric acid was added to 120 μl of homogenate, thoroughly mixed, and centrifuged (10 min; 12,000 × *g*). Using a refrigerated autoinjector, 20 μl of the supernatant was applied to a reverse-phase HPLC column (HR-80; ESA) perfused isocratically at 1 ml/min with a mobile phase consisting of 1.5% acetonitrile, 0.9% triethylamine, 0.59% phosphoric acid, 0.27 mM sodium EDTA, and 8.9 mM heptane sulfonic acid. In the eluate, 3-hydroxykynurenine was detected electrochemically (Coulochem; ESA) at an oxidation potential of +0.2 V (25).

(v) Measurement of dopamine and its acidic metabolites. Striatal tissue was dissected on ice and homogenized in 100 μl of HPLC-grade water. Fifty microliters of the homogenate was then diluted (1:1, vol/vol) with 0.2 M $HClO_4$ and centrifuged for 10 min at 12,000 × *g*. The supernatant was further diluted 1:25 (vol/vol) with a mobile phase consisting of 90 mM KH_2PO_4, 50 mM citric acid, 2.5 mM octane sulfonic acid, 50 μM sodium EDTA, and 8% acetonitrile, pH 3.0. Dopamine, homovanillic acid (HVA), and 3,4-dihydroxyphenylacetic acid (DOPAC) were separated using a reverse-phase HPLC column (MD-150; ESA) perfused isocratically at 1.2 ml/min with the mobile phase. All compounds were detected electrochemically at an oxidation potential of +0.48 V (2).

(vi) Protein measurement. Protein was determined in appropriate aliquots of tissue homogenate using the method of Lowry et al. (34).

Histology. (i) Nissl, glial fibrillary acidic protein (GFAP), and Fluoro Jade B staining. Mice of various ages (PND 7, PND 14, PND 21, 2 months, and 18 months; $n = 2$ each for mutant and wild-type animals per age group) were deeply anesthetized with avertin (600 mg/kg of body weight, intraperitoneally). The brains of PND 7 mice were removed from the skull and fixed by immersion in fixative (4% paraformaldehyde in 0.1 M phosphate buffer; pH 7.4). Older animals were perfused transcardially with 0.9% NaCl and fixative. Brains were left in fixative overnight, rinsed in 0.1 M phosphate buffer (pH 7.4; PB), cryoprotected in PB containing 30% sucrose, and frozen using CO_2. Thirty-micrometer tissue sections of the entire brain were cut coronally using a cryostat and collected in PB for the different staining procedures.

Nissl stain, GFAP immunohistochemistry, and Fluoro Jade B staining were performed according to well-established procedures, and every fourth section was analyzed for each method. GFAP antibodies (diluted 1:2,000) were obtained from Zymed (San Francisco, Calif.). Fluoro Jade B was purchased from Histo-Chem Inc. (Jefferson, Ark.) (52).

(ii) Golgi impregnation. The impregnating solution for Golgi staining consisted of 5% $K_2Cr_2O_7$, 4% K_2CrO_4, and 5% $HgCl_2$ in distilled water (39). This solution (1.5 liters) was prepared under low light conditions and stored in an acid-cleaned flask covered with aluminum foil. One liter of distilled water was added at the time when fixed tissue specimens (coronally cut, approximately 2-mm-thick hemibrain blocks from the frontal cortex and striatum; $n = 2$ per experimental group) were prepared for the staining procedure. The tissue blocks were placed in individual acid-cleaned plastic tissue cassettes. Groups of no more than 15 cassettes were placed in gauze suspension bags, and the bags were suspended in the impregnating solution in a 4-liter Erlenmeyer flask. The flask was sealed, covered with foil, and placed on a rotating platform (25 to 30 rpm) for 10 days. On the 11th day, the cassettes were removed, rinsed thoroughly in several changes of distilled water over a 1-h period, and placed in the dark for 6 h in an alkalizing solution (0.5% LiOH and 15% KNO_3 in distilled water). The cassettes were then submerged in 0.2% glacial acetic acid, which was changed and replenished four times during the 18-h immersion period. Finally, the cassettes were washed for 1 h in distilled water (three changes), and the tissues were removed from the cassettes, dehydrated in graded alcohols, and embedded individually in Beem capsules using Spurr's epoxy embedding medium. The medium was polymerized at 60°C overnight. Sections (25 to 30 μm) were cut using a rotary microtome, placed on glass slides, adhered with gentle heating on a warm hot plate, and coverslipped using a low-viscosity mounting medium.

(iii) Quantification of dendritic spines. Golgi-impregnated tissue sections were observed using an Olympus Lab-2 light microscope (bright-field optics) with an attached digital camera, and neurons and dendrites were studied and photographed at a magnification of ×400. For each animal, 12 to 15 fields displaying well-impregnated neurons and dendrites were photographed. Digital images were printed in an 8- by 10-in. format, and each photograph was coded to conceal the identity of the animal. All photographs were randomly arranged and presented to the investigator, who then selected dendrites for evaluation in each of the photographs. Two-centimeter segments (each representing approximately 20 μm of dendritic length) of both primary and secondary dendrites were then marked on each 8-by-10 photograph, and the number of spines was counted and recorded on each marked segment. Subsequently, the code was broken, and the numbers of spines were tabulated.

(iv) Liver histology. Specimens of formalin-fixed liver tissue from mutant and wild-type animals ($n = 2$ per experimental group) were embedded, cut into 6-μm sections, and stained with hematoxylin and eosin, Masson trichrome, or periodic acid-Schiff stain. The sections were then examined by light microscopy to assess cytological and histological features.

Data analysis. An unpaired Student's *t* test was used for any two-group comparison. A one-way or two-way analysis of variance (ANOVA) with appropriate post-hoc analysis was used to compare three or more groups. When the same animals were tested several times, a repeated-measures ANOVA with appropriate post-hoc analysis was used. A P value of <0.05 was considered significant in all analyses.

Analysis of dendritic spine densities was performed using the generalized

estimating equations method for unbalanced repeated measures (33). This method takes account of correlations among repeated counts of dendrites from the same animal using the model of dendrite count = group. Separate analyses of primary and secondary dendrites were conducted for PND 21 and 2-month-old animals. The effect of group was tested at 0.05/4 = 0.0125 to account for multiple testing using a Bonferroni correction.

RESULTS

Generation of *mKat-2*$^{-/-}$ mice. A 768-bp genomic fragment that included exon 2 of the *mKat-2* gene was replaced by a PGKneo cassette in opposite orientation relative to *kat-2* transcription (Fig. 2A). Any *mKat-2* transcript resulting from this genetic modification would result in the truncation of the protein in the *neo* gene, and any transcript that spliced around this modified region would result in a frameshift and protein truncation. Targeted ES cell clones (Fig. 2B) were injected into blastocysts, and three founders were identified that showed germ line transmission of the targeted *mKat-2* allele. Animals in an inbred or a mixed background were generated by mating chimeras with either 129/SvEv or NIH Black Swiss mice, respectively. No phenotypic differences were detected between the mixed and inbred backgrounds in the F1 and F2 generations. F1 heterozygous offspring were intercrossed, and F2 offspring were genotyped by Southern blotting and PCR analyses. All three genotypes (+/+, +/−, and −/−) were detected in the F2 litters (Fig. 2C). Cumulative genotyping of heterozygous crosses yielded the expected Mendelian ratios. To verify that deletion of exon 2 within the *mKat-2* gene resulted in animals null for *mKat-2*, we performed Northern blot analysis using full-length *mKat-2* cDNA as a probe, which demonstrated loss of *mKat-2* transcript in *mKat-2*$^{-/-}$ mice (Fig. 2D). Western analyses using an anti-KAT II polyclonal antibody of protein extracts from kidney revealed the absence of the expected 40-kDa protein in *mKat-2*$^{-/-}$ mice (Fig. 2E).

Perinatal behavioral changes in *mKat-2*$^{-/-}$ mice. No effects on viability, longevity, and fertility were observed in *mKat-2* homozygous null mice. Feeding and grooming behavior were also grossly normal. Likewise, no differences between wild-type and *mKat-2*$^{-/-}$ mice were detected in testing developmental milestones such as surface righting, cliff aversion, negative geotaxis, rooting, forelimb grasp, and auditory startle. However, *mKat-2*$^{-/-}$ mice showed earlier eye opening and precocious acquisition of complex motor behaviors, such as open field crossing and air righting (Table 1).

In the open field arena, *mKat-2*$^{-/-}$ mice displayed increased locomotor activity from PND 17 to PND 26 (Fig. 3). However, this difference was transitory and restricted to this age range, as older animals did not exhibit this hyperactive behavior. Analysis of the videotaped sessions revealed that *mKat-2*$^{-/-}$ mice reared more than wild-type mice. Further quantification of rearing behavior was performed in a separate group of mice using a Digiscan activity monitor, which showed a significantly increased number of horizontal and vertical movements in *mKat-2*$^{-/-}$ animals from PND 17 to PND 30 (data not shown).

Motor coordination in *mKat-2*$^{-/-}$ mice was investigated using an accelerating rotarod apparatus. Mice of both genotypes were able to learn the motor coordination task, as evidenced by an increase in mean latencies during the training and testing period. At PND 21, a significant difference with regard to genotype ($P < 0.05$) was observed. However, this difference diminished in animals that were 2 and 6 months of age (Fig. 4).

TABLE 1. Analysis of neonatal behavior in wild-type and *mKat-2*$^{-/-}$ mice ($n = 8$ per group)

Behavior test	First day of behavior[a]	
	Wild type	*mKat-2*$^{-/-}$
Surface righting	1.5 ± 0.3	1.3 ± 0.2
Cliff aversion	4.9 ± 0.7	5.1 ± 0.5
Negative geotaxis	6.1 ± 0.6	7.1 ± 0.4
Rooting	5.0 ± 0.6	4.6 ± 0.5
Forelimb grasp	7.8 ± 0.2	7.4 ± 0.2
Auditory startle	13.4 ± 0.3	13.0 ± 0.3
Eye opening	13.0 ± 0.0	12.1 ± 0.1*
Open field	12.4 ± 0.2	11.4 ± 0.2*
Air righting	13.1 ± 0.1	12.4 ± 0.3*

[a] Starting from when the animals were born, pups were examined daily for the acquisition of developmental milestones. The values (± SEM) listed represent the first day on which 50% of the pups were able to perform a particular behavior. *, $P < 0.05$ versus wild type (one-way ANOVA).

Normal liver and kidney function in *mKat2*$^{-/-}$ mice. In addition to the brain, *mKat-2* is also highly expressed in liver and kidney (69). In order to examine the effects of loss of *mKat-2* in liver or renal function, blood chemistry analyses were performed in 2- and 9-month-old *mKat-2*$^{-/-}$ and wild-type animals. Liver function, determined by measuring levels of hepatic enzymes, including aspartate aminotransferase, alanine aminotransferase, and γ-glutamyl transpeptidase, along with bilirubin levels, total protein, and albumin, showed no difference between mutant animals and wild-type controls at 2 months (Table 2) and 9 months (data not shown) of age. Examination of renal function revealed similar blood urea nitrogen levels between the groups. Serum creatinine levels in nullizygous animals were significantly lower than in wild-type mice but remained well within normal limits.

Histological examination of liver sections from PND 21 and

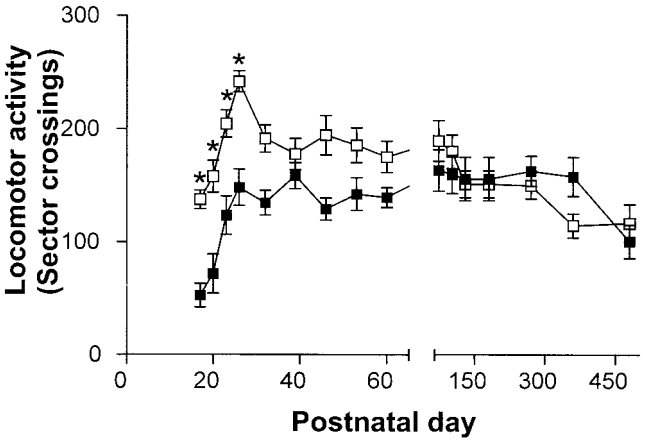

FIG. 3. Locomotor activity in wild-type (solid squares) and *mKat-2*$^{-/-}$ (open squares) mice at various ages. Values represent the number of sector border crossings during the 5-min testing session. The same wild-type ($n = 17$) and *mKat-2*$^{-/-}$ ($n = 18$) mice were used longitudinally. One *mKat-2*$^{-/-}$ mouse died at 5 months, and one *mKat-2*$^{-/-}$ mouse and two wild-type mice died at 10 months. Data are expressed as the mean ± the standard error of the mean. *, $P < 0.05$ versus wild type (two-way ANOVA).

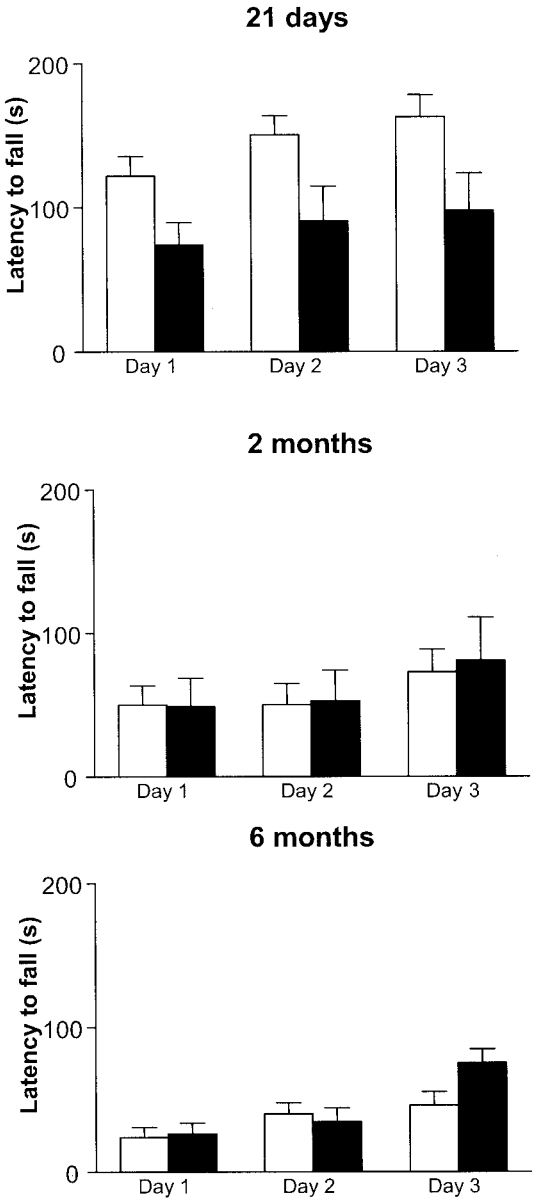

FIG. 4. Motor coordination in wild-type (open bars) and *mKat-2*$^{-/-}$ (solid bars) mice of different ages. Rotarod assessment was performed as described in Materials and Methods ($n = 8$ per experimental group). Data are expressed as the mean ± the standard error of the mean. P was <0.05 versus wild type at PND 21 but not at the other ages (repeated-measures ANOVA).

2-month-old animals showed no differences between *mKat-2*$^{-/-}$ and wild-type mice. All sections that were examined showed normal histologic and cytologic features (micrographs not shown).

Early and transient decreases in brain KAT activity and KYNA levels. Because of the relative importance of KAT II activity in the rat brain (20), we anticipated a substantial and permanent reduction in total cerebral KAT activity in *mKat-2*$^{-/-}$ mice. However brain KAT activity in the mutant mice was moderately decreased at PND 7 and 14 (by 44 and 38%, respectively, compared to age-matched wild-type mice) and returned to normal levels by PND 21 and thereafter (Fig. 5). In contrast, liver KAT activity in the *mKat-2* nullizygous animals was reduced to less than 10% of wild-type activity throughout the entire life span (Fig. 5). Immunoprecipitation with a polyclonal anti-KAT II antibody was then used to further examine the contribution of KAT II to total KAT activity in the mouse brain and liver. These studies were performed using tissues from wild-type mice at PND 7, PND 14, and 2 months of age. In agreement with the results obtained with *mKat-2*$^{-/-}$ mice, antibody-induced elimination of KAT II caused a 46 and 32% decrement in total brain KAT activity in PND 7 and PND 14 mice, respectively. However, total brain KAT in 2-month-old mice was not reduced by antibody treatment. On the other hand, liver KAT was almost totally abolished in all three age groups (Fig. 5). These results suggest that in the mouse, unlike the rat, KAT II accounts for less than 50% of total KAT activity in the brain and that KAT II contribution is maximal during the first weeks of postnatal development. However, in the mouse liver, our data indicate that KAT II is almost exclusively responsible for the transamination of kynurenine to KYNA.

TABLE 2. Analysis of serum samples from 2-month-old wild-type ($n = 6$) and *mKat-2*$^{-/-}$ mice ($n = 6$)[a]

Blood chemistry	Wild type	*mKat-2*$^{-/-}$	Normal range
ALT (U/liter)	68.7 ± 25.1	68.8 ± 14.3	24–140
AST (U/liter)	164.8 ± 64.2	86.3 ± 7.3	72–288
GGT (U/liter)	0.3 ± 0.3	0.0 ± 0.0	0–2
Total bilirubin (mg/dl)	0.1 ± 0.0	0.1 ± 0.1	0–0.9
Direct bilirubin (mg/dl)	0.0 ± 0.0	0.0 ± 0.0	0–0.2
Total protein (g/dl)	4.7 ± 0.1	4.7 ± 0.1	4.0–6.2
Albumin (g/dl)	2.6 ± 0.1	2.7 ± 0.3	2.6–4.6
BUN (mg/dl)	25.5 ± 3.3	23.3 ± 2.4	9–28
Creatinine (mg/dl)	0.3 ± 0.1	0.2 ± 0.0*	0.2–0.7

[a] Samples were obtained as described in the text and commercially analyzed (AniLytics). Analysis of liver and renal function included measurements of aspartate aminotransferase (AST), alanine aminotransferase (ALT), γ- glutamyl transpeptidase (GGT), and blood urea nitrogen (BUN). Data are expressed as the mean ± SEM. *, $P < 0.05$ versus wild type (one-way ANOVA).

Measurements of cerebral and hepatic KYNA levels in *mKat-2*$^{-/-}$ mice compared to age-matched wild-type mice showed reductions that were slightly higher in magnitude than changes in KAT activity. Brain KYNA levels in PND 7, PND14, and PND 21 *mKat-2*$^{-/-}$ mice were significantly reduced (by 48 to 60%) compared to controls but were indistinguishable in older animals (Fig. 6). In contrast, liver KYNA levels in mutant mice were decreased to a much greater extent throughout the animals' life span (Fig. 6). As illustrated in Fig. 7, *mKat-2*$^{-/-}$ mice did not show any significant change in the brain or liver tissue content of associated metabolites (kynurenine, 3-hydroxykynurenine, and quinolinic acid) in all ages examined.

In order to determine if the increased locomotor activity seen in young *mKat-2*$^{-/-}$ mice was caused by abnormal striatal dopamine function (reference 43 and references therein), we compared the striatal levels of dopamine and its acidic metabolites, HVA and DOPAC, in PND 21 wild-type and *mKat-2*$^{-/-}$ mice. As shown in Fig. 8, no significant group differences were found in any of the three dopaminergic markers.

Histochemical, immunohistochemical, and Golgi studies in *mKat-2*$^{-/-}$ mice. Light microscopic analysis of Nissl-stained

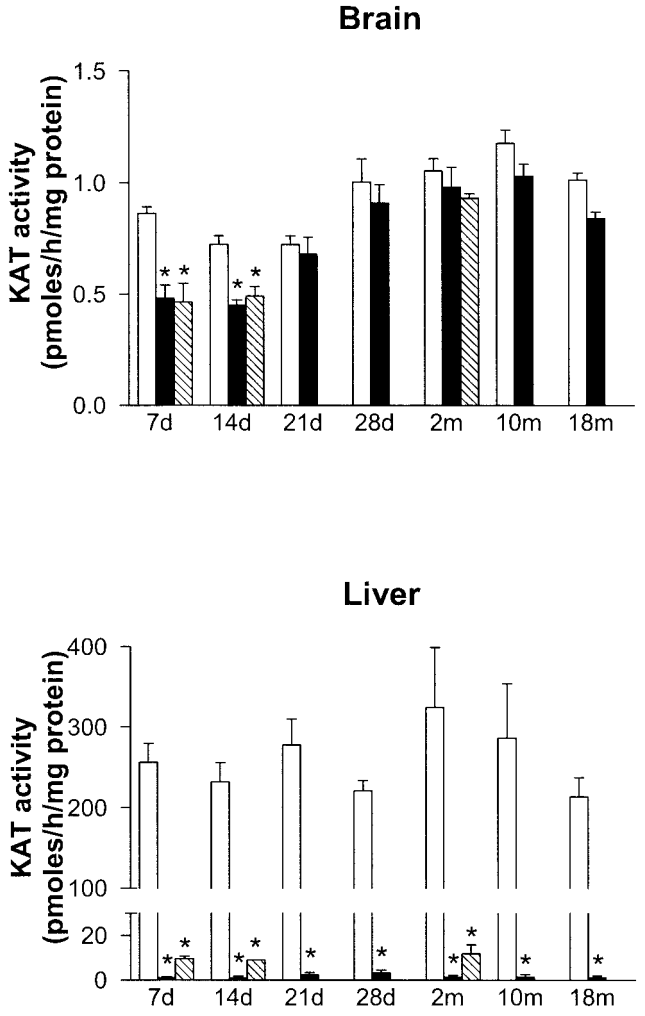

FIG. 5. Total KAT activity in brain and liver of wild-type (open bars) and *mKat-2*$^{-/-}$ (solid bars) mice at various ages. At PND 7, PND 14, and 2 months, anti-KAT II antibodies were used to immunoprecipitate KAT II (hatched bars) in tissues from wild-type mice. See Materials and Methods for experimental details. Data are from four to seven animals per age group and are expressed as the mean ± the standard error of the mean. *, $P < 0.05$ versus wild type (two-way ANOVA). Neither brain nor liver KAT activity differed significantly between *mKat-2*$^{-/-}$ and KAT II-immunoprecipitated wild-type mice at any of the three ages tested.

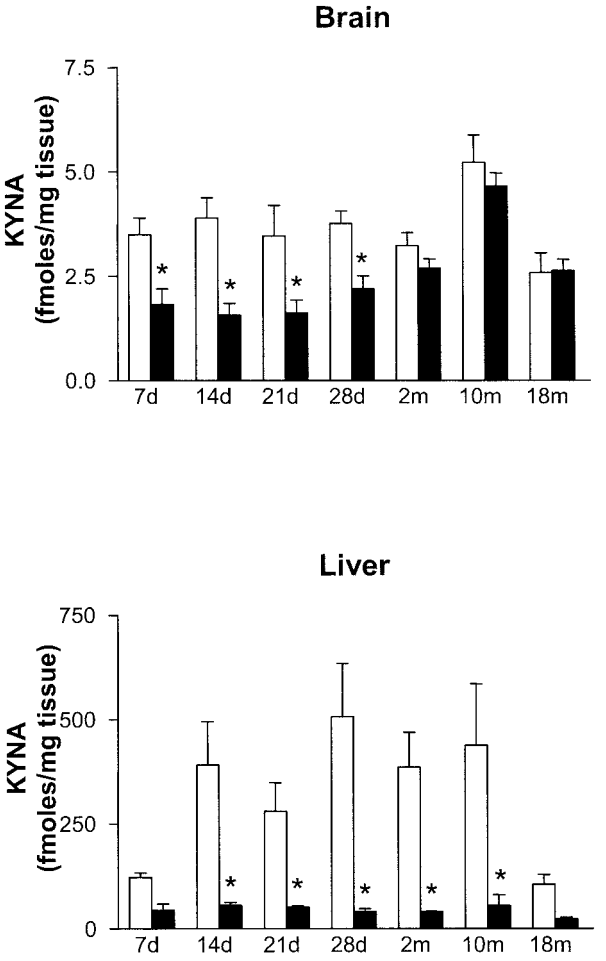

FIG. 6. KYNA levels in brain and liver in wild-type (open bars) and *mKat-2*$^{-/-}$ (solid bars) mice at various ages. Data are from 5 to 12 animals per age group and are expressed as the mean ± the standard error of the mean. *, $P < 0.05$ versus wild type (two-way ANOVA).

brain tissue sections did not reveal obvious abnormalities in the neuronal cytoarchitecture of *mKat-2*$^{-/-}$ mice at the ages examined (micrographs not shown). In addition, tissue sections stained with Fluoro Jade B showed no indication of neuronal degeneration in the brain of *mKat-2*$^{-/-}$ mice at the different ages studied. Moreover, GFAP immunohistochemistry did not reveal any obvious changes in the appearance and distribution of astrocytes in mutant mice compared to control animals. These observations included the analysis of coronal tissue sections throughout the entire rostrocaudal extent of the brain, including the cervical spinal cord (micrographs not shown).

Golgi-stained brain tissue sections from PND 21 and 2-month-old mutant and wild-type mice were examined for comparisons of dendritic morphology. Cortical neurons from PND 21 *mKat-2*$^{-/-}$ mice consistently exhibited dendrites with a more luxuriant proliferation of spines, some of which had a prominently bulbous appearance (cf. Fig. 9A and B). Qualitatively similar abnormalities were observed in dendrites of striatal neurons from PND 21 mutant mice (micrographs not shown). Quantitative assessment of spines on both primary and secondary dendrites of cortical and striatal neurons revealed significantly greater spine densities in PND 21 *mKat-2*$^{-/-}$ mice compared to wild-type controls (both $P < 0.05$) (Table 3). In contrast, no qualitative spine abnormalities were noted in the cortex (cf. Fig. 9C and D) or striatum (micrographs not shown) of 2-month-old *mKat-2*$^{-/-}$ mice. Likewise, there were no quantitative differences observed in spine densities on cortical or striatal neurons from 2-month-old mutant and wild-type animals ($P > 0.4$ for both primary and secondary dendrites) (Table 3).

DISCUSSION

Targeted disruption of the *mKat-2* gene in mice resulted in a marked reduction of KAT activity and, hence, decreased KYNA levels in liver and to a lesser degree in brain, without

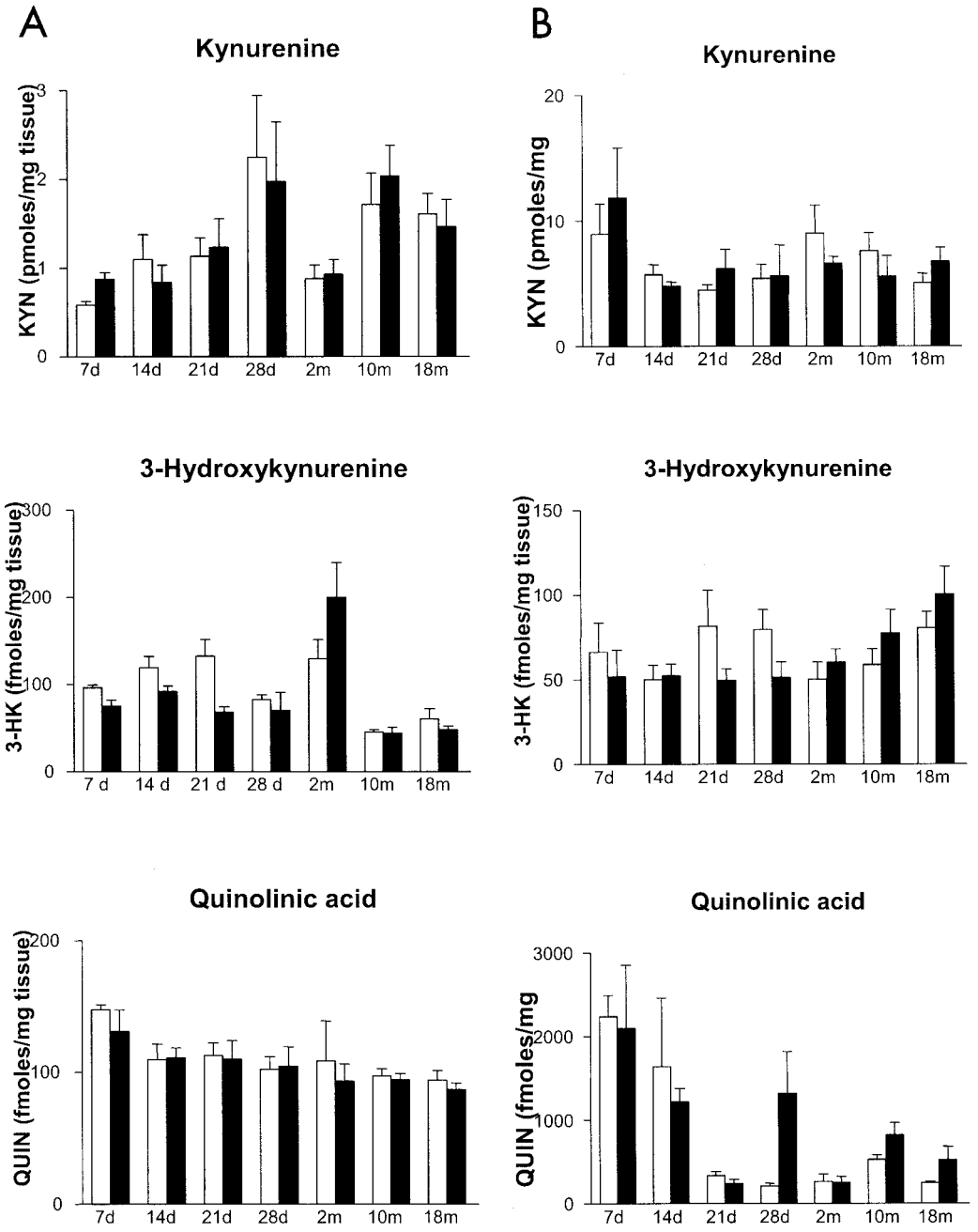

FIG. 7. Brain (A) and liver (B) levels of kynurenine, 3-hydroxykynurenine (3-HK), and quinolinic acid (QUIN) in wild-type (open bars) and *mKat-2*$^{-/-}$ (solid bars) mice at various ages. Data are from 5 to 12 animals per age group and are expressed as the mean ± the standard error of the mean.

affecting the liver or brain content of kynurenine, 3-hydroxykynurenine, and quinolinic acid. In contrast to the liver, which showed a lasting and dramatic KYNA deficit, the decrease in brain KYNA in *mKat-2*$^{-/-}$ mice was limited to the first few weeks of life. This transient period of reduced brain KYNA levels was accompanied by a behavioral phenotype, i.e., hyperlocomotion and decreased motor coordination. Moreover, microscopic analyses revealed significant abnormalities in the appearance and density of dendritic spines in young mutant mice, though no evidence of neurodegeneration or other gross neuropathological changes were observed in brain sections from these animals. After approximately 1 month of age, neuropathological changes reverted to wild-type appearance and density, in parallel with the normalization of brain KAT activity and KYNA levels. Behavioral abnormalities also subsided in *mKat-2*$^{-/-}$ mice after the first month of life. These results demonstrate that disruption of the *mKat-2* gene leads to a transient deficit in brain KYNA levels during the first postnatal

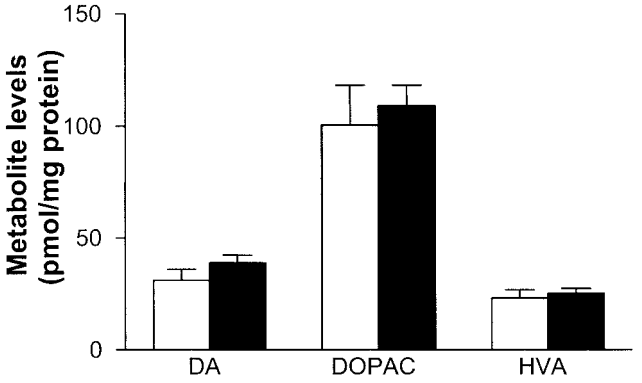

FIG. 8. Levels of dopamine and its acidic metabolites HVA and DOPAC in the striatum of PND 21 wild-type (open bars) and *mKat-2*$^{-/-}$ (solid bars) mice ($n = 7$ per group). Data are expressed as the mean ± the standard error of the mean. Two-way ANOVA revealed no significant differences with respect to genotype.

weeks, coinciding with neuronal and behavioral abnormalities. This would suggest that *mKat-2* expression and function is maximal during the first weeks of postnatal development (Fig. 2F) and that KAT II accounts for less than 50% of total KAT activity in the brain of juvenile mice.

In line with previous reports on pronounced species differences (32), the present study revealed substantial, functionally relevant differences between rat and mouse KAT. In the rat liver, four enzymes are capable of irreversibly converting kynurenine to KYNA, but their relative contributions to KYNA synthesis in vivo are unknown (32). Rat and human brain contain two KATs, arbitrarily termed KAT I and KAT II, which are identical to two of the known peripheral KATs, glutamine aminotransferase K and L-α-aminoadipate aminotransferase, respectively (6, 20, 41). In contrast to KAT I, KAT II has a physiological pH optimum and lacks substrate competition by glutamine, tryptophan, phenylalanine, and other amino acids which are present in the brain in high concentrations. The dramatic reduction in liver KAT activity throughout the mutant animals' life span demonstrated that KAT II is the

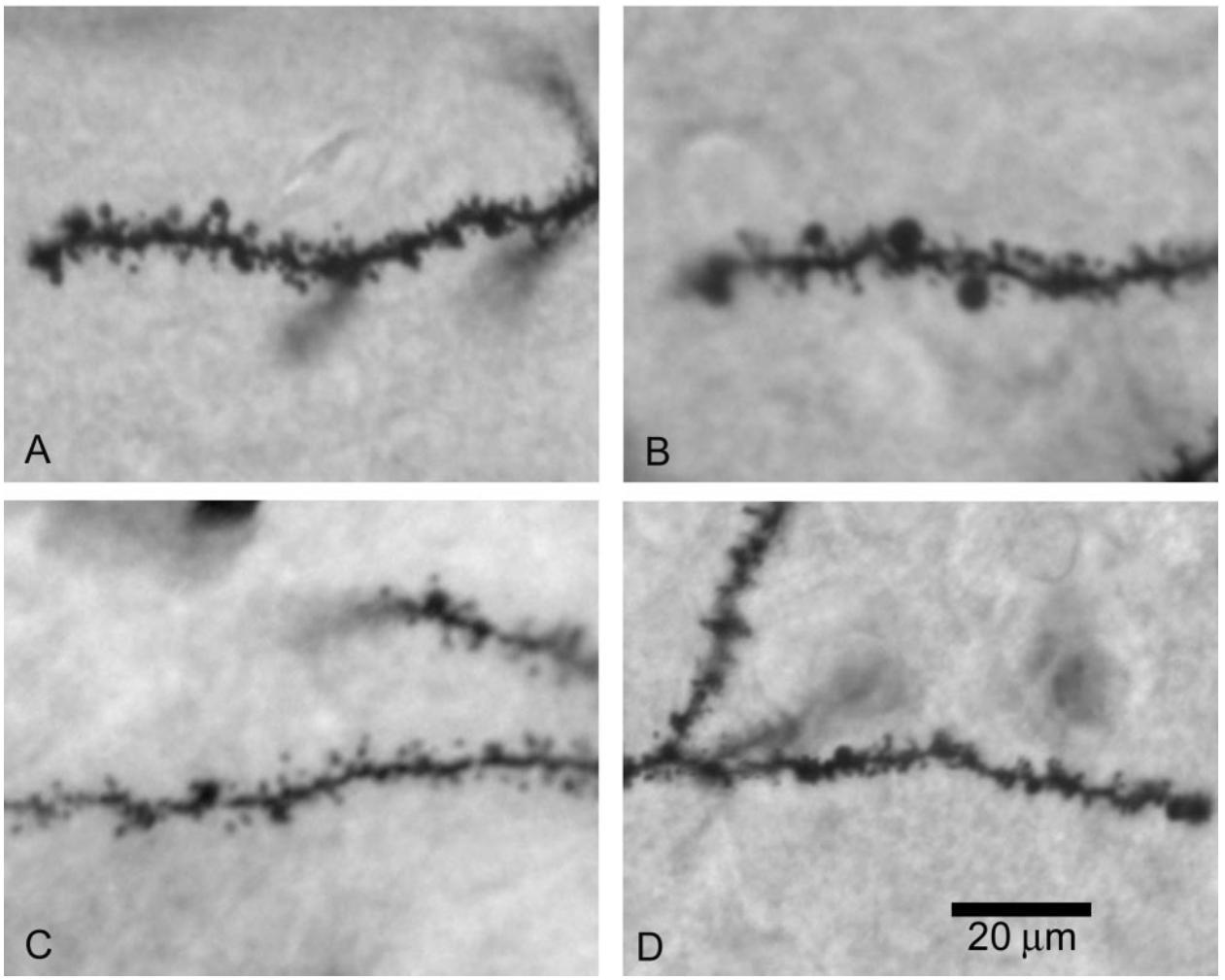

FIG. 9. Representative dendritic morphology of cortical neurons from wild-type and mutant mice, demonstrated by Golgi staining. (A and C) PND 21 and 2-month-old wild-type mice, respectively; (B and D) PND 21 and 2-month-old *mKat-2*$^{-/-}$ mice, respectively. Note that the dendrite in panel B is thicker and that spines are occasionally bulbous in appearance. See Table 3 for quantification of spine densities.

TABLE 3. Quantification of dendritic spines[a]

Sample and age	No. of spines/10-μm dendritic length			
	Primary dendrites		Secondary dendrites	
	Wild type	*mKat-2*$^{-/-}$	Wild type	*mKat-2*$^{-/-}$
Cortex				
PND 21	7.37 ± 0.40	10.07 ± 0.16*	7.81 ± 0.14	9.75 ± 0.58*
2 mo	8.06 ± 0.16	8.22 ± 0.17	7.67 ± 0.12	7.96 ± 0.27
Striatum				
PND 21	9.05 ± 0.27	10.38 ± 0.25*	9.48 ± 0.26	10.79 ± 0.29*
2 mo	9.21 ± 0.30	8.85 ± 0.31	9.52 ± 0.29	9.28 ± 0.25

[a] Quantification of dendritic spines was performed as described in Materials and Methods. Data are the mean ± SEM from 12 to 15 dendrites per experimental group. *, $P < 0.05$ versus wild type. The effect of group was tested at $0.05/4 = 0.0125$ to account for multiple testing using a Bonferroni correction.

dominant hepatic KAT in the mouse. Brain KAT activity in *mKat-2*$^{-/-}$ mice, on the other hand, was only reduced during the first weeks of life, suggesting that the contribution of KAT II to total KAT activity in the normal mouse brain is essentially transient and developmentally regulated. However, it is unlikely that the restored brain KAT activity in 1 month and older *mkat2*$^{-/-}$ mice is due to compensatory KAT I activity, since the assay used in this study discriminates between KAT I (with an optimum pH of 9.5 and which is inhibited by glutamine) and KAT II. This was further substantiated by experiments using anti-KAT II antibodies in liver and brain tissue from wild-type mice, where immunoprecipitation showed a >90% reduction in KAT activity in the liver and more moderate, age-dependent decreases in brain KAT (Fig. 5). Moreover, *mKat-1* developmental expression pattern in brains of wild-type and *mKat-2* knockout mice are not significantly different from each other (Fig. 2G). Thus, the results presented here and the enzymatic properties of KAT I would argue against its major role in cerebral KYNA synthesis in vivo. It is more likely that the mouse brain may contain one or more as-yet-unidentified aminotransferases which are more similar in their properties to KAT II and may be primarily responsible for KYNA formation in the adult mouse brain.

All known KATs have K_m values for kynurenine in the high micromolar or in the millimolar range (32). De novo KYNA formation therefore increases linearly with increased availability of kynurenine, especially under physiological conditions, when substrate concentrations are in the low micromolar range (58, 62, 63). However, the concentration of KYNA in vivo can also be regulated in the absence of fluctuations in kynurenine levels, i.e., by changes in KAT activity. For example, the increases in cerebral KAT expression seen in the aging brain (5, 19) or following experimental brain lesions (9, 68) are accompanied by roughly proportional elevations of KYNA but not kynurenine levels. The present study supports this view, since decreases in brain KAT due to *mKat-2* disruption are associated with quantitatively similar reductions in brain KYNA content without changes in kynurenine levels. Of note, this causal relationship between KAT activity and endogenous KYNA levels is not limited to the brain, as evidenced by the parallel >90% reduction in hepatic KAT activity and KYNA levels in *mKat-2*$^{-/-}$ mice.

Because of the apparent lack of effective mechanisms to control the cellular release of KYNA (63) and because of the absence of degradation and reuptake processes for KYNA (65), changes in intracellular synthesis can cause rapid and proportional fluctuations in extracellular KYNA (18, 30). Even relatively small increases in extracellular KYNA in the brain are functionally significant, resulting in a reduction in extracellular glutamate levels (8). Interestingly, such moderate increases are also anticonvulsant and reduce neuronal vulnerability to ischemic and other excitotoxic insults (7, 12, 24, 36, 45, 51, 53), supporting the possible clinical relevance of fluctuations in brain KYNA.

mKat-2-deficient animals showed transient and relatively modest reductions in cerebral KYNA content in the brain, a feature which correlated with interesting phenotypic changes. Mutant mice did not display apparent abnormal behaviors during the first 2 weeks of postnatal development but showed pronounced hyperactivity and a lack of motor coordination between PND 17 and PND 26. These anomalous behaviors subsided in parallel with the normalization of brain KYNA levels and as the animals matured. Notably, as assessed in the striatum of PND 21 *mKat-2*$^{-/-}$ mice, the changes in motor behavior were not associated with abnormal tissue levels of dopamine, HVA, and DOPAC (Fig. 8) or abnormal dopamine turnover (unpublished data).

The increase in dendritic spine density and the thickened and occasionally bulbous profiles of some spines characteristic of immature spines were conspicuous in PND 21 *mKat-2*$^{-/-}$ mice. However, these features became indistinguishable in 2-month-old mutant and wild-type mice. Since dendritic spines are known to carry nicotinic and NMDA receptors (16, 48, 70), these structural changes may explain recent data demonstrating an increase in α7nAChR function (3) and enhanced vulnerability to quinolinate (M. T. Sapko, P. Yu, P. Guidetti, R. Pellicciari, D. A. Tagle, and R. Schwarcz, Soc. Neurosci. Abstr. **29:**805.20, 2003) in young *mKat-2*$^{-/-}$ mice. Both α7nAChR and NMDA receptors are known to play critical roles in the development and function of dendritic spines (11, 35, 57, 66). It is therefore possible that the changes in spine morphology and density in the young mutant mice are a direct consequence of increased α7nAChR and NMDA receptor function due to the transient reduction in brain levels of the endogenous α7nAChR and NMDA receptor antagonist KYNA. In fact, our group's recent work indicated that the transient decrease in KYNA levels in *mKat-2*$^{-/-}$ mice is sufficient to enhance α7nAChR activity in CA1 stratum radiation interneurons, resulting in increased GABA-ergic synaptic activity of CA1 pyramidal neurons in the hippocampus (3). It is likely that the enhanced spontaneous locomotor activity observed in 21-day-old *mKat-2*$^{-/-}$ mice is a result of increased GABA-ergic activity in the hippocampus similar to that seen in rodents after intrahippocampal microinjection of GABA or its receptor agonists muscimol (3). Importantly, the dendritic changes seen in young *mKat-2*$^{-/-}$ mice were not accompanied by signs of neuronal damage, nor was there any evidence of abnormal neurodegeneration or astrogliosis.

Because of the transient reduction in brain KYNA, the *mKat-2*$^{-/-}$ mouse is an excellent model in which to study the role of KYNA during development and, in particular, to examine its role in the absence of concomitant changes in the quinolinic acid branch of the kynurenine pathway. Moreover, *mKat-2*$^{-/-}$ mice also provide a valuable tool for examining the

role of KYNA and other kynurenines in brain pathology. Abnormalities in cerebral kynurenine pathway metabolism have been identified in several diseases affecting the human brain and may have primary or secondary roles in pathophysiology (59). Pharmacological interventions aimed at normalizing these impairments have been proposed to provide clinical benefits (53, 60). Ongoing studies are therefore designed to further characterize normal and abnormal glutamatergic and cholinergic function in *mKat-2*$^{-/-}$ mice and to use the animals for studying the pathogenesis and treatment of neurological and psychiatric disorders.

ACKNOWLEDGMENTS

This work was supported in part by U.S. Public Health Service grants HD 16596 and NS 25296.

We thank Camille Chung and Tracie Moss for excellent technical assistance, E. Okuno for providing anti-KAT II antibodies, Robert McMahon for expert advice concerning statistical analyses, Kay Washington for consultation on liver pathology, and Vinod Charles and Hemachandra Reddy for valuable discussions. We are also grateful to Sharon Stilling for help with manuscript preparation.

REFERENCES

1. **Abraham, D. G., and A. J. Cooper.** 1996. Cloning and expression of a rat kidney cytosolic glutamine transaminase K that has strong sequence homology to kynurenine pyruvate aminotransferase. Arch. Biochem. Biophys. **335:** 311–320.
2. **Acworth, I. N., and M. L. Cunningham.** 1999. The measurement of monoamine neurotransmitters in microdialysis perfusates using HPLC-ECD. Methods Mol. Med. **22:**219–236.
3. **Alkondon, M., E. F. R. Pereira, P. Yu, E. Z. Arruda, L. E. F. Almeida, P. Guidetti, W. P. Fawcett, M. T. Sapko, W. R. Randall, R. Schwarcz, D. A. Tagle, and E. X. Albuquerque.** 2004. Targeted deletion of the kynurenine aminotransferase II gene reveals a critical role of endogenous kynurenic acid in the regulation of synaptic transmission via α7 nicotinic receptors in the hippocampus. J. Neurosci. **24:**4635–4648.
4. **Beal, M. F., W. R. Matson, K. J. Swartz, P. H. Gamache, and E. D. Bird.** 1990. Kynurenine pathway measurements in Huntington's disease striatum: evidence for reduced formation of kynurenic acid. J. Neurochem. **55:**1327–1339.
5. **Blalock, E. M., K. C. Chen, K. Sharrow, J. P. Herman, N. M. Porter, T. C. Foster, and P. W. Landfield.** 2003. Gene microarrays in hippocampal aging: statistical profiling identifies novel processes correlated with cognitive impairment. J. Neurosci. **23:**3807–3819.
6. **Buchli, R., D. Alberati-Giani, P. Malherbe, C. Köhler, C. Broger, and A. M. Cesura.** 1995. Cloning and functional expression of a soluble form of kynurenine/alpha-aminoadipate aminotransferase from rat kidney. J. Biol. Chem. **270:**29330–29335.
7. **Carpenedo, R., E. Meli, F. Peruginelli, D. E. Pellegrini-Giampietro, and F. Moroni.** 2002. Kynurenine 3-mono-oxygenase inhibitors attenuate post-ischemic neuronal death in organotypic hippocampal slice cultures. J. Neurochem. **82:**1465–1471.
8. **Carpenedo, R., A. Pittaluga, A. Cozzi, S. Attucci, A. Galli, M. Raiteri, and F. Moroni.** 2001. Presynaptic kynurenate-sensitive receptors inhibit glutamate release. Eur. J. Neurosci. **13:**2141–2147.
9. **Ceresoli-Borroni, G., P. Guidetti, and R. Schwarcz.** 1999. Acute and chronic changes in kynurenate formation following an intrastriatal quinolinate injection in rats. J. Neural Transm. **106:**229–242.
10. **Chiarugi, A., E. Meli, and F. Moroni.** 2001. Similarities and differences in the neuronal death processes activated by 3OH-kynurenine and quinolinic acid. J. Neurochem. **77:**1310–1318.
11. **Collin, C., K. Miyaguchi, and M. Segal.** 1997. Dendritic spine density and LTP induction in cultured hippocampal slices. J. Neurophysiol. **77:**1614–1623.
12. **Cozzi, A., R. Carpenedo, and F. Moroni.** 1999. Kynurenine hydroxlyase inhibitors reduce ischemic brain damage: studies with (m-nitrobenzoyl)-alanine and 3,4-dimethoxy-[-N-4-(nitrophenyl)thiazol-2-yl]-benzenesulphonamide (Ro 61–8048) in models of focal or global brain ischemia. J. Cereb. Blood Flow Metab. **19:**771–777.
13. **Crawley, J. N.** 1999. Behavioral phenotyping of transgenic and knockout mice: experimental design and evaluation of general health, sensory functions, motor abilities, and specific behavioral tests. Brain Res. **835:**18–26.
14. **Eastman, C. L., and T. R. Guilarte.** 1989. Cytotoxicity of 3-hydroxykynurenine in a neuronal hybrid cell line. Brain Res. **495:**225–231.
15. **Erhardt, S., K. Blennow, C. Nordin, E. Skogh, L. H. Lindstrom, and G. Engberg.** 2001. Kynurenic acid levels are elevated in the cerebrospinal fluid of patients with schizophrenia. Neurosci. Lett. **313:**96–98.
16. **Fabian-Fine, R., P. Skehel, M. L. Errington, H. A. Davies, E. Sher, M. G. Stewart, and A. Fine.** 2001. Ultrastructural distribution of the α7 nicotinic acetylcholine receptor subunit in rat hippocampus. J. Neurosci. **21:**7993–8003.
17. **Foster, A. C., A. Vezzani, E. D. French, and R. Schwarcz.** 1984. Kynurenic acid blocks neurotoxicity and seizures induced in rats by the related brain metabolite quinolinic acid. Neurosci. Lett. **48:**273–278.
18. **Gramsbergen, J. B. P., P. S. Hodgkins, A. Rassoulpour, W. A. Turski, P. Guidetti, and R. Schwarcz.** 1997. Brain-specific modulation of kynurenic acid synthesis in the rat. J. Neurochem. **69:**290–298.
19. **Gramsbergen, J. B. P., W. Schmidt, W. A. Turski, and R. Schwarcz.** 1992. Age-related changes in kynurenic acid production in rat brain. Brain Res. **588:**1–5.
20. **Guidetti, P., E. Okuno, and R. Schwarcz.** 1997. Characterization of rat brain kynurenine aminotransferases I and II. J. Neurosci. Res. **50:**457–465.
21. **Guidetti, P., P. H. Reddy, D. A. Tagle, and R. Schwarcz.** 2000. Early kynurenergic impairment in Huntington's disease and in a transgenic animal model. Neurosci. Lett. **283:**233–235.
22. **Guidetti, P., and R. Schwarcz.** 1999. 3-Hydroxykynurenine potentiates quinolinate but not NMDA toxicity in the rat striatum. Eur. J. Neurosci. **11:**3857–3863.
23. **Guidetti, P., and R. Schwarcz.** 3-Hydroxykynurenine and quinolinate: pathogenic synergism in early grade Huntington's Disease? *In* G. Allegri Filippini and C. V. L. Costa (ed.), Progress in tryptophan research, in press. Plenum Press, New York, N.Y.
24. **Harris, C. A., A. F. Miranda, J. J. Tanguay, R. J. Boegman, R. J. Beninger, and K. Jhamandas.** 1998. Modulation of striatal quinolinate neurotoxicity by elevation of endogenous brain kynurenic acid. Br. J. Pharmacol. **124:**391–399.
25. **Heyes, M. P., and B. J. Quearry.** 1988. Quantification of 3-hydroxykynurenine in brain by high-performance liquid chromatography and electrochemical detection. J. Chromatogr. **428:**340–344.
26. **Heyes, M. P., K. Saito, A. Lackner, C. A. Wiley, C. L. Achim, and S. P. Markey.** 1998. Sources of the neurotoxin quinolinic acid in the brain of HIV-1-infected patients and retrovirus-infected macaques. FASEB J. **12:** 881–896.
27. **Hill, J. M., I. Gozes, J. L. Hill, M. Fridkin, and D. E. Brenneman.** 1991. Vasoactive intestinal peptide antagonist retards the development of neonatal behaviors in the rat. Peptides **12:**187–192.
28. **Hilmas, C., E. F. R. Pereira, M. Alkondon, A. Rassoulpour, R. Schwarcz, and E. X. Albuquerque.** 2001. The brain metabolite kynurenic acid inhibits α7 nicotinic receptor activity and increases non-α7 nicotinic receptor expression: physiopathological implications. J. Neurosci. **21:**7463–7473.
29. **Hodgkins, P. S., and R. Schwarcz.** 1998. Interference with cellular energy metabolism reduces kynurenic acid formation in rat brain slices: reversal by lactate and pyruvate. Eur. J. Neurosci. **10:**1986–1994.
30. **Hodgkins, P. S., H.-Q. Wu, H. R. Zielke, and R. Schwarcz.** 1999. 2-Oxoacids regulate kynurenic acid production in the rat brain: studies in vitro and in vivo. J. Neurochem. **72:**643–651.
31. **Kessler, M., T. Terramani, G. Lynch, and M. Baudry.** 1989. A glycine site associated with N-methyl-D-aspartic acid receptors: characterization and identification of a new class of antagonists. J. Neurochem. **52:**1319–1328.
32. **Kido, R.** 1984. Kynurenine aminotransferase activity in human and other mammalian tissue, p. 651–656. *In* H. G. Schlossberger, W. Kochen, B. Linzen, and H. Steinhart (ed.), Progress in tryptophan and serotonin research. de Gruyter, Berlin, Germany.
33. **Liang, K. Y., and S. Zeger.** 1986. Longitudinal data analysis using generalized linear models. Biometrika **73:**13–22.
34. **Lowry, O. H., N. J. Rosebrough, A. L. Farr, and R. J. Randall.** 1951. Protein measurement with Folin phenol reagent. J. Biol. Chem. **193:**265–275.
35. **Maletic-Savatic, M., R. Malinow, and K. Svoboda.** 1999. Rapid dendritic morphogenesis in CA1 hippocampal dendrites induced by synaptic activity. Science **283:**1923–1927.
36. **Miranda, A. F., R. J. Boegman, R. J. Beninger, and K. Jhamandas.** 1997. Protection against quinolinic acid-mediated excitotoxicity in nigrostriatal dopaminergic neurons by endogenous kynurenic acid. Neuroscience **78:**967–975.
37. **Moroni, F., P. Russi, G. Lombardi, M. Beni, and V. Carla.** 1988. Presence of kynurenic acid in the mammalian brain. J. Neurochem. **51:**177–180.
38. **Mosca, M., L. Cozzi, J. Breton, C. Speciale, E. Okuno, R. Schwarcz, and L. Benatti.** 1994. Molecular cloning of rat kynurenine aminotransferase: identity with glutamine transaminase K. FEBS Lett. **353:**21–24.
39. **Moss, T. L., and W. O. Whetsell, Jr.** Techniques for thick-section Golgi impregnation of formalin-fixed brain tissue. *In* Y. Kohwi (ed.), Methods in molecular biology, in press. Humana Press, Totowa, N.J.
40. **Okuda, S., N. Nishiyama, H. Saito, and H. Katsuki.** 1996. Hydrogen peroxide-mediated neuronal cell death induced by an endogenous neurotoxin, 3-hydroxykynurenine. Proc. Natl. Acad. Sci. USA **93:**12553–12558.
41. **Okuno, E., M. Nakamura, and R. Schwarcz.** 1991. Two kynurenine aminotransferases in human brain. Brain Res. **542:**307–312.

42. **Okuno, E., M. Tsujimoto, M. Nakamura, and R. Kido.** 1993. 2-Aminoadipate-2-oxoglutarate aminotransferase isoenzymes in human liver: a plausible physiological role in lysine and tryptophan metabolism. Enzyme Protein **47:**136–148.
43. **Onn, S. P., A. R. West, and A. A. Grace.** 2000. Dopamine-mediated regulation of striatal neuronal and network interactions. Trends Neurosci. **10**(Suppl.)**:**S48–S56.
44. **Pearson, S. P., and G. P. Reynolds.** 1992. Increased brain concentrations of a neurotoxin, 3-hydroxykynurenine, in Huntington's disease. Neurosci. Lett. **144:**199–201.
45. **Pellicciari, R., B. Natalini, G. Costantino, M. R. Mahamoud, L. Mattoli, B. M. Sadeghpour, F. Moroni, A. Chiarugi, and R. Carpenedo.** 1994. Modulation of the kynurenine pathway in search for new neuroprotective agents. Synthesis and preliminary evaluation of (m-nitrobenzoyl)alanine, a potent inhibitor of kynurenine 3-hydroxylase. J. Med. Chem. **37:**647–655.
46. **Perkins, M. N., and T. W. Stone.** 1982. An iontophoretic investigation of the actions of convulsant kynurenines and their interaction with the endogenous excitant quinolinic acid. Brain Res. **247:**184–187.
47. **Poeggeler, B., A. Rassoulpour, P. Guidetti, H.-Q. Wu, and R. Schwarcz.** 1998. Dopaminergic control of kynurenate levels and NMDA toxicity in the developing rat striatum. Dev. Neurosci. **20:**146–153.
48. **Racca, C., F. A. Stephenson, P. Streit, J. D. Roberts, and P. Somogyi.** 2000. NMDA receptor content of synapses in stratum radiatum of the hippocampal CA1 area. J. Neurosci. **20:**2512–2522.
49. **Rassoulpour, A., H.-Q. Wu, B. Poeggeler, and R. Schwarcz.** 1998. Systemic *d*-amphetamine administration causes a reduction of kynurenic acid levels in rat brain. Brain Res. **802:**111–118.
50. **Sardar, A. M., J. E. Bell, and G. P. Reynolds.** 1995. Increased concentrations of the neurotoxin 3-hydroxykynurenine in the frontal cortex of HIV-1-positive patients. J. Neurochem. **64:**932–935.
51. **Scharfman, H. E., P. S. Hodgkins, S.-C. Lee, and R. Schwarcz.** 1999. Quantitative differences in the effects of de novo produced and exogenous kynurenic acid in rat brain slices. Neurosci. Lett. **274:**111–114.
52. **Schmued, L. C., and K. J. Hopkins.** 2000. Fluoro-Jade B: a high affinity fluorescent marker for the localization of neuronal degeneration. Brain Res. **874:**123–130.
53. **Schwarcz, R., and R. Pellicciari.** 2002. Manipulation of brain kynurenines: glial targets, neuronal effects and clinical opportunities. J. Pharmacol. Exp. Ther. **303:**1–10.
54. **Schwarcz, R., A. Rassoulpour, H.-Q. Wu, D. Medoff, C. A. Tamminga, and R. C. Roberts.** 2001. Increased cortical kynurenate content in schizophrenia. Biol. Psych. **50:**521–530.
55. **Schwarcz, R., W. O. Whetsell, Jr., and R. M. Mangano.** 1983. Quinolinic acid: an endogenous metabolite that causes axon-sparing lesions in rat brain. Science **219:**316–318.
56. **Shi, L., S. H. Fatemi, R. W. Sidwell, and P. H. Patterson.** 2003. Maternal influenza infection causes marked behavioral and pharmacological changes in the offspring. J. Neurosci. **23:**297–302.
57. **Shoop, R. D., E. Esquenazi, N. Yamada, M. H. Ellisman, and D. K. Berg.** 2002. Ultrastructure of a somatic spine mat for nicotinic signaling in neurons. J. Neurosci. **22:**748–756.
58. **Speciale, C., H.-Q. Wu, J. B. P. Gramsbergen, W. A. Turski, U. Ungerstedt, and R. Schwarcz.** 1990. Determination of extracellular kynurenic acid in the striatum of unanesthetized rats: effect of aminooxyacetic acid. Neurosci. Lett. **116:**198–203.
59. **Stone, T. W.** 2001. Kynurenines in the CNS: from endogenous obscurity to therapeutic importance. Prog. Neurobiol. **64:**185–218.
60. **Stone, T. W., and L. G. Darlington.** 2002. Endogenous kynurenines as targets for drug discovery and development. Nat. Rev. Drug Discov. **1:**609–620.
61. **Stone, T. W., and M. N. Perkins.** 1981. Quinolinic acid: a potent endogenous excitant at amino acid receptors in CNS. Eur. J. Pharmacol. **72:**411–412.
62. **Swartz, K. J., M. J. During, A. Freese, and M. F. Beal.** 1990. Cerebral synthesis and release of kynurenic acid: an endogenous antagonist of excitatory amino acid receptors. J. Neurosci. **10:**2965–2973.
63. **Turski, W. A., J. B. P. Gramsbergen, H. Traitler, and R. Schwarcz.** 1989. Rat brain slices produce and liberate kynurenic acid upon exposure to L-kynurenine. J. Neurochem. **52:**1629–1636.
64. **Turski, W. A., M. Nakamura, W. P. Todd, B. K. Carpenter, W. O. Whetsell, Jr., and R. Schwarcz.** 1988. Identification and quantification of kynurenic acid in human brain tissue. Brain Res. **454:**164–169.
65. **Turski, W. A., and R. Schwarcz.** 1988. On the disposition of intrahippocampally injected kynurenic acid in the rat. Exp. Brain Res. **71:**563–567.
66. **Woolley, C. S., N. G. Weiland, B. S. McEwen, and P. A. Schwartzkroin.** 1997. Estradiol increases the sensitivity of hippocampal CA1 pyramidal cells to NMDA receptor-mediated synaptic input: correlation with dendritic spine density. J. Neurosci. **17:**1848–1859.
67. **Wu, H.-Q., A. Rassoulpour, and R. Schwarcz.** 2002. Effect of systemic L-dopa administration on extracellular kynurenate levels in the rat striatum. J. Neural Transm. **109:**239–249.
68. **Wu, H.-Q., U. Ungerstedt, and R. Schwarcz.** 1992. Regulation of kynurenic acid synthesis studied by microdialysis in the dorsal hippocampus of unanesthetized rats. Eur. J. Pharmacol. **213:**375–380.
69. **Yu, P., D. M. Mosbrook, and D. A. Tagle.** 1999. Genomic organization and expression analysis of mouse kynurenine aminotransferase II, a possible factor in the pathophysiology of Huntington's disease. Mamm. Genome **10:**845–852.
70. **Yuste, R., A. Majewska, and K. Holthoff.** 2000. From form to function: calcium compartmentalization in dendritic spines. Nat. Neurosci. **7:**653–659.